



Published in final edited form as:

Nat Med. 2011 June ; 17(6): 726–731. doi:10.1038/nm.2380.

Defective Wnt-dependent cerebellar midline fusion in a mouse model of Joubert syndrome

Madeline A. Lancaster^{1,4}, Dipika J. Gopal¹, Joon Kim¹, Sahar N. Saleem², Jennifer L. Silhavy¹, Carrie M. Louie¹, Bryan E. Thacker¹, Yuko Williams¹, Maha S. Zaki³, and Joseph G. Gleeson^{1,*}

¹ Laboratory for Neurogenetics, Howard Hughes Medical Institutes, Department of Pediatrics and Neurosciences, Institute for Genomic Medicine, University of California, San Diego

² Radiology Department, Kasr Al-Ainy Hospital, Cairo University, Cairo, Egypt

³ Clinical Genetics Department, Human Genetics and Genome Research Division, National Research Centre, Cairo, Egypt

Abstract

The ciliopathy Joubert syndrome is marked by cerebellar vermis hypoplasia, a phenotype for which the pathogenic mechanism is unclear^{1–3}. In order to investigate Joubert syndrome pathogenesis, we have examined mice with mutated *Ahi1*, the first identified Joubert syndrome gene^{4,5}. These mice exhibit cerebellar hypoplasia with a vermis/midline fusion defect early in development. This defect is concomitant with expansion of the roof plate and is also evident in a mouse mutant for another Joubert syndrome gene, *Cep290*^{6,7}. Further, fetal magnetic resonance imaging (MRI) from human subjects with Joubert syndrome reveals a similar midline cleft suggesting parallel pathogenic mechanisms. Previous evidence has suggested a role for Joubertin (Jbn), the protein encoded by *Ahi1*, in canonical Wnt signaling⁸. Consistent with this, we found decreased Wnt reporter activity at the site of hemisphere fusion in the developing cerebellum of *Ahi1* mutant mice. This decrease was accompanied by reduced proliferation at the site of fusion. Finally, treatment with lithium, a Wnt pathway agonist⁹, partially rescued this phenotype. Our findings implicate a defect in Wnt signaling in the cerebellar midline phenotype seen in Joubert syndrome, which can be overcome with Wnt stimulation.

Keywords

Neuroscience; signaling; Wnt; ataxia; cerebellum; cilia; Joubert syndrome; Joubertin; Ahi1

Users may view, print, copy, download and text and data- mine the content in such documents, for the purposes of academic research, subject always to the full Conditions of use: http://www.nature.com/authors/editorial_policies/license.html#terms

*Address for correspondence: jogleeson@ucsd.edu, LBR 482, 9500 Gilman Dr., University of California, San Diego, La Jolla, CA 92093-0665, Tel: 858-822-3535, Fax: 858-822-1021.

⁴Current address: IMBA - Institute of Molecular Biotechnology of the Austrian Academy of Science, Vienna, Austria

Author contributions. J.G.G. and M.A.L. conceived and designed the experimental approach, interpreted data, and wrote the manuscript. M.A.L. and D.J.G. carried out *in vivo* characterization experiments. M.A.L. performed *in vitro* Wnt assays. J.K. and Y.W. designed and generated *Cep290* mutant mice. S.N.S. and M.H.Z. performed patient diagnosis and provided patient MRIs. J.L.S. generated constructs and materials for *in vitro* assays. C.M.L. and B.T. contributed to *in vivo* characterizations. J.G.G. directed and supervised the project.

Competing financial interests statement. The authors declare no competing financial interests

Joubert syndrome is a developmental disorder marked by cerebellar vermis hypoplasia and a unique molar tooth sign on imaging (MTI)^{2,3}, and is part of a larger spectrum of disorders known as ciliopathies. Although the primary cilium seems to be involved in pathogenesis of these disorders, its exact function within this context is not clear. Some hints have come from conditional cilia mouse mutants which exhibit similar ciliopathy phenotypes, including cerebellar hypoplasia^{10,11}. However, the resulting cerebellar phenotypes appear more severe than those seen in Joubert syndrome, suggesting a more specific defect may be to blame in the human disease. Recent evidence has identified several key signaling pathways that rely on or are regulated by cilia, such as Wnt and Shh signaling^{12,13}. Since mouse mutants for genes null mutated in Joubert syndrome have not yet been examined for cerebellar phenotypes, the mechanism of Joubert syndrome pathogenesis in cerebellar vermis formation is still not clear.

In order to study mechanisms of Joubert syndrome pathogenesis, we examined a mouse model of loss of function of *Ahil*, mutated in Joubert syndrome and encoding the Jbn protein^{4,5}. Adult *Ahil*^{-/-} mice exhibited smaller body size as reported previously¹⁴ with slightly reduced brain size compared with *Ahil*^{+/-} or *Ahil*^{+/+} mice, which were indistinguishable from each other. Overall brain morphology of *Ahil*^{-/-} mice appeared normal except for a smaller cerebellum and underdeveloped vermis with a mildly defective foliation pattern¹⁵ (Fig. 1a). Vermian lobules VI and VII appeared fused while lobule V appeared smaller and underdeveloped at 3 weeks of age. Overall, the cerebellum appeared slightly hypoplastic suggesting a developmental defect that may be similar to Joubert syndrome though much less severe in the mouse.

We next examined cresyl-violet stained midline sagittal sections which revealed that although the overall brain size was reduced by 17% compared with controls (Supplementary Fig. 1a) the cerebellar vermis appeared more severely affected as it was reduced by 40% (Fig. 1b), and this decrease was more statistically significant when corrected for total brain size, which decreased the variance (Supplementary Fig. 1a). Furthermore, foliation defects in lobules V, VI and VII were also visible on sagittal sections similar to that seen on whole-mount (Fig. 1b). *Ahil*^{-/-} mice consistently displayed an average decrease in number of folia of 1.5 compared with littermate controls (Fig. 1c). Additionally, these size and foliation defects persisted beyond three weeks, throughout adulthood (Supplementary Fig. 1b).

Although the MTI is present in humans with Joubert syndrome, no evidence of this sign was present in mouse mutants (Supplementary Fig. 1c). Additionally, other defects described in Joubert syndrome such as fragmentation of deep cerebellar nuclei and structural anomalies of the descending trigeminal tract and brainstem nuclei^{16,17} were not evident in *Ahil* mutants (Supplementary Fig. 1c, d). Decussation of pyramidal axons, which can be abnormal in humans with Joubert syndrome^{16,17}, also appeared normal in *Ahil* mutants (Supplementary Fig. 1e). Furthermore, despite the cerebellar defects, cellular organization and layering appeared normal in *Ahil* mutant mice compared with littermate controls (Supplementary Fig. 2a). Additionally, staining for the Purkinje neuron marker Calbindin and the granule neuron marker GABA-A receptor $\alpha 6$ revealed intact cell fate and layering

(Supplementary Fig. 2b). Finally, Golgi-Cox stain revealed normal neuronal morphology within the adult cerebellum of mutant mice (Supplementary Fig. 2c).

We next examined cerebellar development in *Ahi1* mutants. At postnatal day five (P5), transverse sections revealed a vermal foliation defect with an overall smaller vermis in *Ahi1*^{-/-} mice (Fig. 1d). Similarly, sagittal sections at P4 revealed a smaller cerebellar vermis size and underdeveloped foliation with lobules V, VI and VII most affected (Fig. 1e). At E18.5, a very subtle size defect was evident (Fig. 1e). The size defect was also quantified at E18.5 and P4 (Fig. 1f).

Since both foliation and size are dependent upon expansion of cerebellar neurons, this phenotype could be due to defects in proliferation. We therefore tested BrdU staining in cerebellar granule neurons (CGNs) of the developing cerebellar midline. We examined several stages from E16.5 to P5 and detected a significant decrease in CGN BrdU staining within the vermis at E16.5, which recovered by E18.5 and remained equivalent at most postnatal time points, though a slight but significant decrease was evident at P5 (Fig. 2a, b). However, isolated P5 CGNs from *Ahi1*^{-/-} and control mice did not exhibit a difference when labeled with BrdU *in vitro* (data not shown). The proliferation defect at E16.5 could also be detected by phospho-histone H3 staining *in vivo* to detect cells in mitosis (Supplementary Fig. 3a). This suggests a relatively early defect in proliferation of CGN precursors.

One of the major regulatory pathways in CGN proliferation is Shh signaling; however, this pathway is primarily active at postnatal time points¹⁸. Since cilia regulate Shh signaling, and Joubert syndrome is a ciliopathy, we nevertheless tested for a Shh defect in these mice. We stained sections from P2 *Ahi1*^{-/-} and *Ahi1*^{+/-} littermates for N-myc, a proliferative gene target of Shh signaling (Fig. 2c). N-myc staining appeared strongest in CGNs, as reported previously¹⁹, and was not decreased in *Ahi1*^{-/-} cerebella. Furthermore, western blot analysis of N-myc protein levels from whole cerebellum lysates at P3 revealed equal levels in *Ahi1*^{-/-} mouse cerebellum compared with littermate control (Supplementary Fig. 3b). We also stained for an independent Shh target gene, Patched (Ptc1), and observed similar levels of expression in *Ahi1* mutant mice (Supplementary Fig. 3c). Finally, we performed qRT-PCR for three Shh target genes: N-Myc, Gli1, and Ptc1, and did not observe any differences in expression in *Ahi1*^{-/-} mice compared with littermate controls (Fig. 2d). We can therefore conclude that postnatal Shh signaling appears intact in *Ahi1* mutant cerebella. We further tested Shh signaling at earlier time points as described below.

Given the early proliferation defect, we next examined morphology of the developing cerebellum at earlier embryonic stages. Transverse sections from *Ahi1*^{-/-} embryos revealed a striking midline fusion defect at the cerebellar vermis primordium compared with control littermates (Fig. 3a). This defect was most evident at E16.5 when control vermis had nearly completely fused whereas *Ahi1*^{-/-} vermis was thinner and malformed. The defect was also clearly visible at E14.5 in *Ahi1*^{-/-} brain compared with control littermate. Whole mount images of embryos at E12.5 (Fig. 3b) also revealed a separation of developing cerebellar hemispheres at the midline with expansion of the rhombic roof plate.

To further examine this roof plate abnormality, we examined sagittal sections from an independent set of E12.5 embryonic brains (Fig. 3c). Serial midline and paramedial sections revealed a lengthened roof plate in *Ahi1*^{-/-} brain compared with littermate control. Furthermore, transverse sections at E13.5 (Supplementary Fig. 4) revealed an overall widened roof plate in the *Ahi1* mutant as visualized by serial sections from anterior to posterior. Matched anterior sections at the site of cerebellar hemisphere fusion revealed defective fusion in *Ahi1* mutant brain compared with control. These findings suggest the cerebellar phenotype may be a result of defective midline fusion with expansion of the roof plate, likely a secondary effect of incomplete growth of midline cerebellar tissue.

Since these studies were aimed at modeling Joubert syndrome, we tested whether these findings were also apparent in an alternate Joubert syndrome model: null mice for *Cep290*, the second gene positionally cloned in Joubert syndrome^{6,7}. Because the only published *Cep290* mutant mouse is the *rd16* line, an in frame deletion without a cerebellum defect²⁰, we decided to target *Cep290* to completely inactivate the gene. We generated *Cep290*^{-/-} mice by targeted homologous recombination (Supplementary Fig. 5a). Although *Cep290* has been described as a key cilia protein in other contexts²¹, *Cep290*^{-/-} mice appeared overall healthy with some runting and a retinal phenotype as in *rd16* mice (data not shown). We nevertheless examined E16.5 *Cep290*^{-/-} mice for possible midline fusion defects. Similar to *Ahi1* mutants, *Cep290*^{-/-} mice exhibited defective midline fusion at E16.5 that was slightly milder than the *Ahi1* phenotype (Fig. 3d). Additionally, adult *Cep290* mutants exhibited a mild foliation defect, although the vermis was not statistically smaller than controls (Supplementary Fig. 5b).

To test whether an early midline fusion defect may be a precursor to Joubert syndrome in humans, we examined fetal MRI from human subjects later verified to have Joubert syndrome. In human development, cerebellar hemispheres fuse at the midline by 13 weeks gestational age (GA) to eventually develop into the vermis²². We were able to obtain MRIs from three subjects with Joubert syndrome between 21 and 25 weeks GA when fusion should be complete. However, fetuses with Joubert syndrome exhibited a striking separation of cerebellar hemispheres at the midline when compared to control MRI (Fig. 3e). Furthermore, this defect was most severe on inferior axial images where there was an apparent connection between the fourth ventricle and the cisterna magna. Similarly, in both *Ahi1*^{-/-} and *Cep290*^{-/-} mice, midline fusion appeared most defective on inferior (more posterior) transverse sections (Fig. 3d and Supplementary Fig. 5c). Finally, it is important to point out that 21–25 weeks GA in humans corresponds to a stage in cerebellar development after fusion occurs (13 weeks in humans, E13.5 in mice). Thus, although the human imaging is consistent with an early fusion defect, it may also be compatible with other early developmental defects leading up to the phenotype seen here. However, the similarities between the human and mouse phenotypes, and their common underlying genetics, suggest these findings are consistent with an early fusion defect in humans with Joubert syndrome.

We next tested the function of several *AHI1* disease mutations to examine mechanisms of Joubert syndrome pathogenesis. We generated tagged plasmid based expression constructs encoding Jbn with one of three disease missense mutations: R723Q and H896R, in the WD40 domain, and V443D, adjacent to a putative atypical PKC phosphorylation site^{4,23,24}.

These disease mutations each exhibited comparable protein expression levels to wild-type Jbn in 293T cells (Supplementary Fig. 6a) and mouse inner medullary collecting duct (IMCD) cells (Supplementary Fig. 6b). We next examined localization and found that all three mutations failed to localize to the primary cilium compared with wild-type Jbn (Supplementary Fig. 6c).

Since Jbn has been identified as a positive modulator of canonical Wnt signaling⁸, we next tested whether these disease mutation constructs were defective in modulation of Wnt activity. We performed luciferase assays with the Super Topflash Wnt reporter construct and treated cells with Wnt3A conditioned media. Overexpression of wild-type Jbn in these cells resulted in a 1.6-fold increase in reporter activity over vector control (Supplementary Fig. 7a). In contrast, none of the mutants exhibited significantly increased Wnt activity compared with control.

Since we previously reported that Jbn interacts with β -catenin⁸, we tested the ability of GFP-tagged disease mutations to co-immunoprecipitate with β -catenin. This approach revealed an interaction between wild-type Jbn and β -catenin as well as an interaction with the R723Q and H896R mutations (Supplementary Fig. 7b). V443D however exhibited a considerable decrease in pulldown of endogenous β -catenin. Although soluble protein levels varied between mutant and wild-type Jbn constructs, immunoprecipitation efficiencies were indistinguishable among disease mutations, indicating a specific reduction in interaction between β -catenin and mutation V443D. Since V443 is adjacent to a putative atypical PKC phosphorylation site, this site may be important for β -catenin interaction.

Since Joubert syndrome is a ciliopathy, we next tested whether Jbn localizes to cilia in CGNs. CGNs isolated from P5 wild-type mouse cerebella exhibited cilia during the first 24 hours following dissociation (Supplementary Fig. 7c). Transfection with Jbn-GFP or staining for endogenous Jbn revealed localization to the basal body in CGNs. We additionally tested β -catenin colocalization by examining β -catenin-GFP and endogenous β -catenin, which exhibited colocalization with Jbn at the base of the cilium.

These findings point to a possible role for the primary cilium in Jbn's Wnt modulatory role. We therefore tested whether primary cilia were disrupted in *Ahi1*^{-/-} CGNs. CGNs isolated from *Ahi1* null and control littermates exhibited indistinguishable number of cilia and morphology (Supplementary Fig. 8a) similar to that recently described in the kidney⁸ and retina¹⁴ of *Ahi1*^{-/-} mice. These results suggest that Jbn is not required for ciliogenesis but perhaps functions more specifically in ciliary-mediated signaling.

Several canonical Wnt mouse mutants exhibit roof plate expansion and vermal defects²⁵⁻²⁷. Given Jbn's previously described Wnt role, and our findings with disease mutations, we tested whether *Ahi1*^{-/-} mice exhibited defective Wnt signaling. We crossed *Ahi1*^{+/-} mice to Wnt reporter BATgal transgenic mice²⁸. We previously reported that *Ahi1* and BATgal are genetically linked⁸. Therefore, in order to generate these mice, we performed backcrossings of *Ahi1*^{+/-}; BATgal+ mice to *Ahi1*^{+/-} mice in order to recover mice with recombined alleles. Since midline fusion begins at approximately E13.5^{29,30}, we examined E13.5 *Ahi1*^{-/-}; BATgal+ embryos for Wnt defects compared with *Ahi1*^{+/-}; BATgal+ littermates. Whole

mount imaging revealed a decrease in Wnt signaling at the cerebellar midline anlage (Fig. 4a). Further examination by transverse sectioning revealed a specific decrease in Wnt activity in cerebellar cells surrounding the midline in mutant tissue. We also examined Shh signaling during midline fusion, by staining for Gli1 and Ptc1. We observed very low-level expression of both factors, which appeared equally low in the *Ahi1* mutant (Supplementary Fig. 8b). These results were not surprising since Shh has been described to be largely absent at this time and Shh defects have not been linked to cerebellar midline fusion defects.

We next hypothesized that, since Wnt is a known mitogen, the tissue expansion at the midline may be due to a mitogenic role for Wnt signaling in this context. We examined proliferation of cerebellar precursors surrounding the site of fusion by performing BrdU pulse labeling. Control littermate embryos exhibited specific labeling of precursors immediately surrounding the fusion site while *Ahi1*^{-/-} embryos exhibited significantly fewer labeled cells in this region (Fig. 4b, c). Furthermore, staining for Arl13b, a cilia marker, revealed a concentration of cilia at the site of fusion (Supplementary Fig. 8c) suggesting Jbn's role may be most important in these ciliated cells. However, cilia in *Ahi1*^{-/-} mice appeared indistinguishable from those of littermate controls, consistent with a role for Jbn in ciliary signaling rather than ciliogenesis.

We next performed a series of experiments using the Wnt agonist lithium to activate Wnt signaling⁹ in *Ahi1*^{-/-} mice. We performed intraperitoneal injections of LiCl, or NaCl as a control, in pregnant dams³¹ at E12.5 and then again at E13.5 and examined E14.5 morphology. We also verified an increase in Wnt signaling with LiCl compared with those treated with NaCl (Supplementary Fig. 9a). At E14.5, *Ahi1*^{-/-} receiving NaCl exhibited midline fusion defects as expected. However, *Ahi1*^{+/-} and *Ahi1*^{-/-} embryos that received LiCl were indistinguishable from each other, suggesting a rescue of the phenotype (Fig. 4d). Interestingly, LiCl treated embryos exhibited expanded cerebellar hemisphere tissue with less of a separation between hemispheres, consistent with the hypothesis that canonical Wnt signaling promotes expansion of hemisphere tissue. However, fusion itself was not enhanced in embryos treated with LiCl suggesting a separate regulatory mechanism for this specific process of midline fusion.

To quantify these effects, we measured extent of midline fusion and proliferation in embryos treated with LiCl. Pregnant dams were again injected with LiCl at E12.5 and E13.5 and embryos were examined at E14.5. We examined expansion of midline tissue by quantification of the size of the ventricular space between hemispheres from at least three mice of each genotype for each condition. This approach revealed a significantly larger inter-hemispheric space in untreated *Ahi1* mutants compared with littermate control mice, while with lithium treatment there was no significant difference between mutants and controls (Fig. 4e). To examine proliferation in these mice, we additionally performed staining for Ki67, which revealed a significant decrease in the number of proliferating cells at the site of fusion of untreated *Ahi1*^{-/-} embryos compared with control littermates whereas lithium treatment rescued this phenotype (Fig. 4f and Supplementary Fig. 9b).

We next performed lithium treatments at E12.5 and E13.5 and examined morphology at later time points. At E16.5, midline morphology of *Ahi1*^{-/-} was indistinguishable from controls,

reflecting intact midline fusion, though the lateral aspect still appeared slightly reduced in size (Fig. 4d). Furthermore, mice examined after birth at P4, revealed a partial rescue of the size and foliation defects in *Ahi1* mutants, which more closely matched untreated controls compared with untreated mutants (Fig. 4g). However, mutant mice still exhibited runting and early postnatal lethality suggesting further treatment or other approaches may be needed to rescue this aspect the phenotype. Additionally, controls that received LiCl also exhibited slightly more advanced development of the vermis compared with untreated mice suggesting activation of Wnt signaling during midline fusion may enhance cerebellar development. Finally, examination of *Ahi1* mutants at P11 revealed slightly more complex foliation and increased size with lithium treatment compared with untreated mutants (Supplementary Fig. 9c). Overall, we have examined five mutants at postnatal time points from P2 to P11 and observe a partial rescue of cerebellar developmental defects when treated with lithium.

We describe for the first time two animal models of Joubert syndrome that provide the first indication that the midline cerebellar hypoplasia seen in this disorder is due to a decrease in Wnt signaling, which can be rescued with lithium treatment. Based on our results with *Ahi1* mutants, we propose a model of the events that occur during midline fusion, disrupted in Joubert syndrome (Supplementary Fig. 10a). Midline fusion from E12.5 to E16.5 occurs with tissue growth at the midline that progressively fills in both posteriorly and ventrally. Rescue experiments with lithium treatments suggest that vermis formation may reflect a combination of at least two processes. First, the surrounding tissue expands due to Wnt dependent proliferation. Second, cells at the midline fuse through an as yet undefined process, which likely involves cell migration and intercalation. Wnt pathway mutations have been identified in cerebellar cancer, termed medulloblastoma³², but an endogenous role for Wnt signaling in cerebellar precursor proliferation had not previously been identified. The early Wnt-dependent proliferation at the midline described here, is at least one key step that is abnormal in Joubert syndrome mutants. This proliferation defect can be mathematically modeled using our observations from BrdU pulse labeling experiments, which reveals a fit with a 2-stage model of proliferation during cerebellar development: an early Wnt-dependent stage and a later Shh-dependent stage (Supplementary Fig. 10b and Supplementary Discussion).

The *Ahi1* and *Cep290* phenotypes are relatively mild in comparison to genes required for ciliogenesis^{10,11}. This, along with the cilia staining in *Ahi1* mutants, suggests that rather than an overall ciliogenesis defect, Joubert syndrome may reflect a more specific defect in cilia function or signaling. Both *Jbn* and *Cep290* have been implicated in transport at the cilium^{14,33,34} and *Jbn* has already been shown to function in nuclear β -catenin transport⁸. Perhaps deficient transport of signaling components such as β -catenin is responsible for more specific downstream signaling defects. Additionally, although Shh signaling appeared largely intact, we cannot rule out possible roles in other signaling pathways important for cerebellum development, such as BMP³⁵, Notch³², and FGF³⁶ signaling pathways, and it will be interesting to examine possible roles for the cilium in these pathways. Overall, these results provide the first insight into a precise mechanism of Joubert syndrome pathogenesis and a unique process of midline fusion involving proliferation followed by tissue fusion. We propose that it is the proliferative phase that is defective in Joubert syndrome and leads to

hypoplasia of the cerebellar vermis. Future studies, as well as more complete evaluations, will be needed to test whether Wnt pathway modulators, such as lithium, may represent a promising candidate treatment in Joubert syndrome.

Online Methods

Plasmid constructs and materials

We generated disease mutation constructs using the QuikChange Site-Directed Mutagenesis Kit (Stratagene). β -catenin-GFP construct was obtained from K. Willert and Jbn-GFP was used as previously described⁸. We obtained Wnt3a conditioned media from L cells stably transfected with Wnt3a expression construct as previously described⁸.

Generation of mouse lines

Ahi1^{-/-} mice were described previously and we crossed heterozygotes to BATgal+ mice (kindly provided by S. Piccolo)²⁸. We generated *Cep290* null mice by targeted homologous recombination to generate a conditional allele (loxP-flanked, 'flox'). The floxed region (containing exons 36 and 37 of 52 exons) and flanking homology arms of *Cep290* were PCR-amplified from 129/SvJ genomic DNA, flanked with SalI, BamHI and XhoI restriction sites, and subcloned into the modified pflox vector³⁷ (from J. Marth) containing PGKneobpA (positive selection) and HSV-TK (negative selection). This was linearized with SbfI and transfected into 129SvJ-derived ES cells. We selected G418- and gancyclovir-resistant clones and injected these into C57Bl/6 blastocysts. High-percentage chimeras were bred to C57Bl/6 for germline transmission and to EIIa-Cre to generate mosaic Cre recombinants, which were bred to C57Bl/6 to isolate mice with null alleles. We confirmed null mice to be absent *Cep290* protein (data not shown). We genotyped mice by PCR in two reactions, one amplifying a 370-bp (null allele) and the other a 414-bp (wild-type) product. Null allele primers were *Cep290*KO-F1: 5'-GGCTCACTGTGATCTTGTGC-3', *Cep290*KO-R2: 5'-TGGAAGACCAGGCTTCAGAG-3', and wild-type primers were *Cep290*WT-F2: 5'-GTAAGTGCCCGACAGCTACC-3', *Cep290*WT-R2: 5'-AGCGCAGTGCAGAGTATGTG-3'. Mouse work was carried out in compliance with Institutional Animal Care and Use Committee approved protocols.

Research subjects

Brain MRI analysis was completed during the clinical assessment of pregnancies at risk for developing Joubert syndrome (based on previously affected older sibling with clinically and radiologically proven Joubert syndrome) using standard sequence protocols at Cairo University (MRI unit in Kasr Al-Ainy Hospital)³⁸. One representative MRI at 25 weeks GA from a patient later confirmed to exhibit Joubert syndrome is provided as well as a control MRI at 25 weeks GA. We obtained parental written informed consent from all families, and the study was approved by the Human Research Protection Program Committees of UCSD (La Jolla) and Cairo University (Egypt).

Histology and immunohistochemistry

We obtained brain sections by perfusion fixation followed by embedding in 10%/7.5% gelatin/sucrose and cryosectioning at 20 μ m thickness, stained for cresyl-violet and imaged

for morphology. Size measurements were performed in a blinded manner using ImageJ to find edges and quantify area from midline (for cerebellar vermis size) and para-medial (for total brain size) sections of each of three mice for each genotype: *Ahi1*^{-/-}, *Cep290*^{-/-} or littermate controls. We quantified foliation by counting the number of lobules as designated by complete separation with intervening molecular layer. We performed X-gal staining identically between control and mutant tissues as previously described for 1–3 hours on whole mount or sections⁸. We stained littermates in parallel in the same X-gal solution. We performed BrdU labeling by injecting pregnant dams or neonatal pups intraperitoneally with 100 µg g⁻¹ body weight of BrdU from a stock solution of 10 mg ml⁻¹ in normal saline. We dissected brains and fixed one hour after BrdU injection. Cells labeled with BrdU or Ki67 were counted from images identically acquired and counted in a blinded manner. We performed intraperitoneal injections of equimolar LiCl or NaCl (10 µl of a 600 mM stock solution in normal saline per gram body weight³¹) in timed pregnant dams at E12.5 and again at E13.5. Golgi-Cox staining used the FD Rapid GolgiStain kit (FD NeuroTechnologies) according to manufacturer

We carried out immunostaining of sections or isolated cells by blocking in 4% donkey serum in 0.1% TritonX, followed by staining with the following primary antibodies: acetylated tubulin (Zymed 32-2700, 1:500 dilution), rabbit antibody to Jbn⁸ (1:500), rabbit antibody to β-catenin (Cell Signaling, 95825, 1:200), rat antibody to Brdu (Abcam, ab6326, 1:200), n-myc (Cell Signaling, 9405, 1:200), chicken antibody to β-galactosidase (Abcam, ab9361, 1:250), rabbit antibody to calbindin (Swant, D28K, 1:250), rabbit antibody to GABA-A receptor α6 (Chemicon, AB5610, 1:500), rat antibody to Ptc1 (R&D systems, MAB41051, 1:100), rabbit antibody to Gli1 (Chemicon, AB3444, 1:200), rabbit antibody to Arl13b (1:1500, gift from T. Caspary), rabbit antibody to Ki67 (1:200, Novocastra, NCL-Ki67p), and rabbit antibody to PH3 (Upstate, 06–570, 1:200). For Jbn staining, we performed antigen retrieval by heating samples in 100 mM Tris, 5% urea, pH9.5 at 95 °C for 10 min. Samples were then washed in PBS and stained with the following secondary antibodies: AlexaFluor donkey antibody to mouse 594, donkey antibody to rat 488, donkey antibody to rabbit 488, goat antibody to rabbit 350, (Molecular Probes, 1:500). Hoechst (Molecular Probes, H3570) was used as the nuclear stain. We isolated CGNs according to a previously published protocol³⁹ and fixed in 4% PFA 5 h after plating onto poly-D-lysine coated slides followed by washing, blocking, and staining. We performed transfection of CGNs with GFP constructs using Amaxa nucleofector primary neuron kit according to manufacturer's protocol. We carried out transfection of Jbn disease mutation GFP constructs in IMCDs using Lipofectamine 2000 (Invitrogen) according to manufacturer's guidelines. We acquired and quantified images using a DeltaVision Spectris deconvolution or a FV1000 Spectral Deconvolution Confocal microscope (UCSD Neuroscience Microscopy Core).

Western blotting and luciferase

We performed western blotting on lysates prepared in modified RIPA buffer using the following antibodies: N-myc (Cell Signaling, 9405), mouse antibody to β-catenin (BD Transduction Labs, 610153), goat antibody to GAPDH (Santa Cruz Biotech, SC-20357), mouse antibody to GFP (Covance, B34), rabbit antibody to TFIID (Santa Cruz Biotech., SC-293), and mouse antibody to α-tubulin (Sigma, T-6074). All antibodies were used at

1:1000 dilution. Rabbit antibody to GFP (Genetex, Gtx26556, 1 μ g) was used for immunoprecipitations from modified RIPA lysates using protein A sepharose beads. For transient transfections of fibroblasts or IMCDs, we used Lipofectamine 2000 (Invitrogen) according to manufacturer's protocol. For luciferase assays, we grew fibroblasts in 12-well plates and transfected with 600 ng Topflash, 120 ng β Gal, and 650 ng of Jbn expression plasmid, empty vector, or disease mutation construct (all containing GFP that we mutated at Y66G to disrupt fluorescence and avoid cross activity with luminescence, using QuikChange mutagenesis). 24 h following transfection, cells were serum starved for 8 h then treated overnight with Wnt3a conditioned media diluted 3:1 in serum free media. We performed the luciferase assay according as previously published⁸ and we measured β -galactosidase activity using the Tropix Galacto-light Plus kit (Applied Biosystems, T1007).

Quantitative RT-PCR

We isolated cerebella from three mice of each genotype, *Ahi1*^{-/-} and littermate controls, at P1 and RNA was extracted using Trizol reagent (Invitrogen). This was used to make cDNA using Superscript III (Invitrogen) according to manufacturer. We performed quantitative PCR in triplicate for each sample and each gene assayed using LightCycler 480 Sybr Green (Roche). We performed analysis using instrument software to obtain crossing point values. Averages were then normalized to values for actin. For statistical analyses, Student's *t*-test was performed to compare knock-out to littermate control values for all quantitative assays. Error bars are S.E.M.

BDA Tracing Assay

We stereotactically injected the anterograde tracer, biotinylated dextran amine (BDA) into layer V of the right sensorimotor cortex of adult *Ahi1*^{+/+} and *Ahi1*^{-/-} mice ($n = 2$ per genotype) following previously established methods⁴⁰. We then sacrificed mice 3 weeks later and prepared 20 μ m cryosections, which were stained with DAB (3,3'-Diaminobenzidine) to visualize labeled CST fibers.

Supplementary Material

Refer to Web version on PubMed Central for supplementary material.

Acknowledgments

We are grateful to members of the Gleeson lab for technical expertise and feedback and B. Hamilton, M. Hatten, and A. Joyner for helpful discussions on cerebellar development. We also thank the patients and the UCSD Neuroscience Microscopy Core. We thank J.K. Lee and B. Zheng for help with BDA tracing assay. We are grateful to S. Piccolo at the Departments of Histology, Microbiology and Medical Biotechnologies, University of Padua, Italy for the BATgal mice. We thank R.T. Moon at the Department of Pharmacology, University of Washington for the Super Topflash construct and K. Willert for stably transfected L cells and β -catenin expression plasmid. M.A.L. received support from the Bear Necessities Pediatric Cancer Foundation and US National Institutes of Health–National Institute of General Medical Sciences–funded UCSD Genetics Training Program (T32 GM08666). This work was supported by the US National Institutes of Health, and the Burroughs Wellcome Fund in Translational Research (J.G.G.). J.G.G. is an investigator with Howard Hughes Medical Institute.

References

1. Badano JL, Mitsuma N, Beales PL, Katsanis N. The ciliopathies: an emerging class of human genetic disorders. *Annu Rev Genomics Hum Genet.* 2006; 7:125–148. [PubMed: 16722803]
2. Joubert M, Eisenring JJ, Robb JP, Andermann F. Familial agenesis of the cerebellar vermis. A syndrome of episodic hyperpnea, abnormal eye movements, ataxia, and retardation. *Neurology.* 1969; 19:813–825. [PubMed: 5816874]
3. Louie CM, Gleeson JG. Genetic basis of Joubert syndrome and related disorders of cerebellar development. *Hum Mol Genet.* 2005; 14(2):R235–242. [PubMed: 16244321]
4. Dixon-Salazar T, et al. Mutations in the AHI1 gene, encoding joubertin, cause Joubert syndrome with cortical polymicrogyria. *Am J Hum Genet.* 2004; 75:979–987. [PubMed: 15467982]
5. Ferland RJ, et al. Abnormal cerebellar development and axonal decussation due to mutations in AHI1 in Joubert syndrome. *Nat Genet.* 2004; 36:1008–1013. [PubMed: 15322546]
6. Valente EM, et al. Mutations in CEP290, which encodes a centrosomal protein, cause pleiotropic forms of Joubert syndrome. *Nat Genet.* 2006; 38:623–625. [PubMed: 16682970]
7. Sayer JA, et al. The centrosomal protein nephrocystin-6 is mutated in Joubert syndrome and activates transcription factor ATF4. *Nat Genet.* 2006; 38:674–681. [PubMed: 16682973]
8. Lancaster MA, et al. Impaired Wnt-beta-catenin signaling disrupts adult renal homeostasis and leads to cystic kidney ciliopathy. *Nat Med.* 2009; 15:1046–1054. [PubMed: 19718039]
9. Hedgepeth CM, et al. Activation of the Wnt signaling pathway: a molecular mechanism for lithium action. *Dev Biol.* 1997; 185:82–91. [PubMed: 9169052]
10. Chizhikov VV, et al. Cilia proteins control cerebellar morphogenesis by promoting expansion of the granule progenitor pool. *J Neurosci.* 2007; 27:9780–9789. [PubMed: 17804638]
11. Spassky N, et al. Primary cilia are required for cerebellar development and Shh-dependent expansion of progenitor pool. *Dev Biol.* 2008; 317:246–259. [PubMed: 18353302]
12. Berbari NF, O'Connor AK, Haycraft CJ, Yoder BK. The primary cilium as a complex signaling center. *Curr Biol.* 2009; 19:R526–535. [PubMed: 19602418]
13. Lancaster MA, Gleeson JG. The primary cilium as a cellular signaling center: lessons from disease. *Curr Opin Genet Dev.* 2009; 19:220–229. [PubMed: 19477114]
14. Louie CM, et al. AHI1 is required for photoreceptor outer segment development and is a modifier for retinal degeneration in nephronophthisis. *Nat Genet.* 42:175–180. [PubMed: 20081859]
15. Cooper PA, Benno RH, Hahn ME, Hewitt JK. Genetic analysis of cerebellar foliation patterns in mice (*Mus musculus*). *Behav Genet.* 1991; 21:405–419. [PubMed: 1953602]
16. Yachnis AT, Rorke LB. Neuropathology of Joubert syndrome. *J Child Neurol.* 1999; 14:655–659. discussion 669–672. [PubMed: 10511338]
17. Friede RL, Boltshauser E. Uncommon syndromes of cerebellar vermis aplasia. I: Joubert syndrome. *Dev Med Child Neurol.* 1978; 20:758–763. [PubMed: 729929]
18. Corrales JD, Rocco GL, Blaess S, Guo Q, Joyner AL. Spatial pattern of sonic hedgehog signaling through Gli genes during cerebellum development. *Development.* 2004; 131:5581–5590. [PubMed: 15496441]
19. Kenney AM, Cole MD, Rowitch DH. Nmyc upregulation by sonic hedgehog signaling promotes proliferation in developing cerebellar granule neuron precursors. *Development.* 2003; 130:15–28. [PubMed: 12441288]
20. Chang B, et al. In-frame deletion in a novel centrosomal/ciliary protein CEP290/NPHP6 perturbs its interaction with RPGR and results in early-onset retinal degeneration in the rd16 mouse. *Hum Mol Genet.* 2006; 15:1847–1857. [PubMed: 16632484]
21. Craig B, et al. CEP290 tethers flagellar transition zone microtubules to the membrane and regulates flagellar protein content. *J Cell Biol.* 2010; 190:927–940. [PubMed: 20819941]
22. ten Donkelaar HJ, Lammens M, Wesseling P, Thijssen HO, Renier WO. Development and developmental disorders of the human cerebellum. *J Neurol.* 2003; 250:1025–1036. [PubMed: 14504962]
23. Parisi MA, et al. AHI1 mutations cause both retinal dystrophy and renal cystic disease in Joubert syndrome. *J Med Genet.* 2006; 43:334–339. [PubMed: 16155189]

24. Valente EM, et al. AHI1 gene mutations cause specific forms of Joubert syndrome-related disorders. *Ann Neurol.* 2006; 59:527–534. [PubMed: 16453322]
25. Thomas KR, Musci TS, Neumann PE, Capecchi MR. Swaying is a mutant allele of the proto-oncogene Wnt-1. *Cell.* 1991; 67:969–976. [PubMed: 1835670]
26. Schuller U, Rowitch DH. Beta-catenin function is required for cerebellar morphogenesis. *Brain Res.* 2007; 1140:161–169. [PubMed: 16824494]
27. Louvi A, Alexandre P, Metin C, Wurst W, Wassef M. The isthmic neuroepithelium is essential for cerebellar midline fusion. *Development.* 2003; 130:5319–5330. [PubMed: 14507778]
28. Maretto S, et al. Mapping Wnt/beta-catenin signaling during mouse development and in colorectal tumors. *Proc Natl Acad Sci U S A.* 2003; 100:3299–3304. [PubMed: 12626757]
29. Cheng LE, Zhang J, Reed RR. The transcription factor Zfp423/OAZ is required for cerebellar development and CNS midline patterning. *Dev Biol.* 2007; 307:43–52. [PubMed: 17524391]
30. Millen KJ, Wurst W, Herrup K, Joyner AL. Abnormal embryonic cerebellar development and patterning of postnatal foliation in two mouse *Engrailed-2* mutants. *Development.* 1994; 120:695–706. [PubMed: 7909289]
31. Cohen ED, et al. Wnt signaling regulates smooth muscle precursor development in the mouse lung via a tenascin C/PDGFR pathway. *J Clin Invest.* 2009; 119:2538–2549. [PubMed: 19690384]
32. Marino S. Medulloblastoma: developmental mechanisms out of control. *Trends Mol Med.* 2005; 11:17–22. [PubMed: 15649818]
33. Hsiao YC, et al. Ahi1, whose human ortholog is mutated in Joubert syndrome, is required for Rab8a localization, ciliogenesis and vesicle trafficking. *Hum Mol Genet.* 2009; 18:3926–3941. [PubMed: 19625297]
34. Kim J, Krishnaswami SR, Gleeson JG. CEP290 interacts with the centriolar satellite component PCM-1 and is required for Rab8 localization to the primary cilium. *Hum Mol Genet.* 2008; 17:3796–3805. [PubMed: 18772192]
35. Grimmer MR, Weiss WA. BMPs oppose Math1 in cerebellar development and in medulloblastoma. *Genes Dev.* 2008; 22:693–699. [PubMed: 18347086]
36. Yaguchi Y, et al. Fibroblast growth factor (FGF) gene expression in the developing cerebellum suggests multiple roles for FGF signaling during cerebellar morphogenesis and development. *Dev Dyn.* 2009; 238:2058–2072. [PubMed: 19544582]
37. Koizumi H, Tanaka T, Gleeson JG. Doublecortin-like kinase functions with doublecortin to mediate fiber tract decussation and neuronal migration. *Neuron.* 2006; 49:55–66. [PubMed: 16387639]
38. Saleem SN, Zaki MS. Role of MR imaging in prenatal diagnosis of pregnancies at risk for Joubert syndrome and related cerebellar disorders. *AJNR Am J Neuroradiol.* 31:424–429. [PubMed: 19942698]
39. Hatten ME. Neuronal regulation of astroglial morphology and proliferation in vitro. *J Cell Biol.* 1985; 100:384–396. [PubMed: 3881455]
40. Lee J, et al. Reassessment of corticospinal tract regeneration in Nogo-deficient mice. *J Neurosci.* 2009; 29:8649–8654. [PubMed: 19587271]

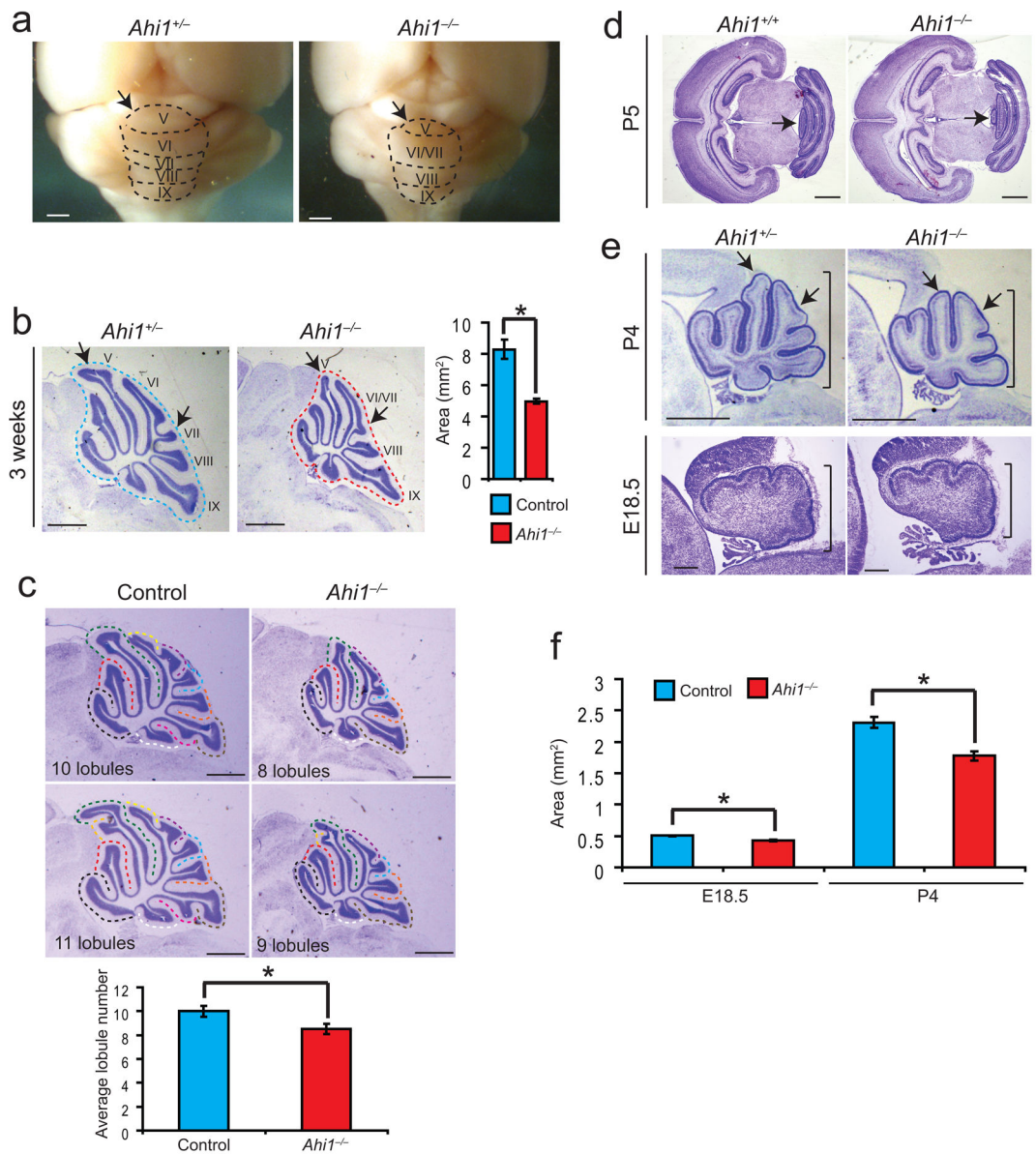


Figure 1. Reduced cerebellum size and foliation defects in *Ahi1*^{-/-} mice

(a) Whole mount images of representative mutant and littermate control brains. The vermal folia are outlined with dashed lines and the visible folia V-IX are labeled. Scale bar, 1 mm. (b) Midline sagittal cresyl-violet (C-V) stained sections from representative littermates. Folia are labeled and arrows indicate foliation defects: decreased size of V and fusion of VI and VII. Scale bar, 1 mm. Quantification of vermis area at the right showing average area measurements of midline sections. * $P < 0.05$, Student's t -test, $n = 3$ for each genotype. (c) Quantification of foliation defects in *Ahi1* mutant mice. Lobules were identified and counted from six mice for each genotype, *Ahi1*^{-/-} and control, and the average is shown below. * $P < 0.05$, Student's t -test. Scale bar, 1 mm. (d) Transverse C-V stained sections from P5 littermates revealing specific vermis folia size defect particularly in folia V (arrows). Scale bar, 1 mm. (e) Sagittal midline C-V stained sections from representative littermates aged P4

and E18.5 revealing the presence of a mild size defect (bars) and foliation defects (arrows). Scale bar, 1 mm (upper panels), 200 μm (lower panels). (f) Average vermis area at E18.5 and P4 in *Ahi1*^{-/-} and control littermates. * $P < 0.05$, Student's *t*-test, $n = 3$ for each genotype. Error bars are S.E.M.

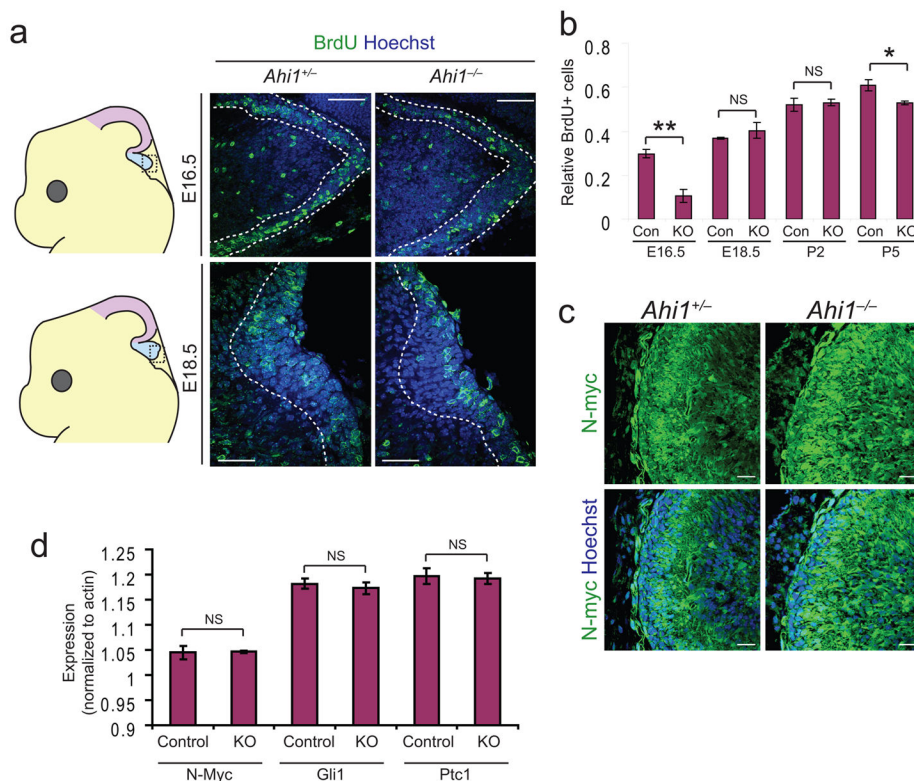


Figure 2. Early proliferation defect and the absence of a postnatal Shh defect

(a) BrdU stained (green) sections from representative littermates aged E16.5 and E18.5. Dashed lines demarcate external granule layer and Hoechst labels nuclei. Scale bar, 50 μ m. (b) Quantification of BrdU labeled CGNs indicated as average number of BrdU positive cells as a ratio of total CGNs. E16.5, and to a lesser extent P5, reveal a significant decrease in relative BrdU stained cells. * $P < 0.05$, ** $P < 0.005$ Student's *t*-test, $n = 3$ for each genotype. (c) N-myc staining (green) in midline sagittal sections from P5 littermates. Hoechst labels nuclei. Scale bar, 20 μ m (d) qRT-PCR analysis of Shh target genes, N-Myc, Gli1, and Ptc1. Values are average expression levels relative to actin. NS=not significant, Student's *t*-test, $n = 3$ for each genotype and gene tested. Error bars are S.E.M.

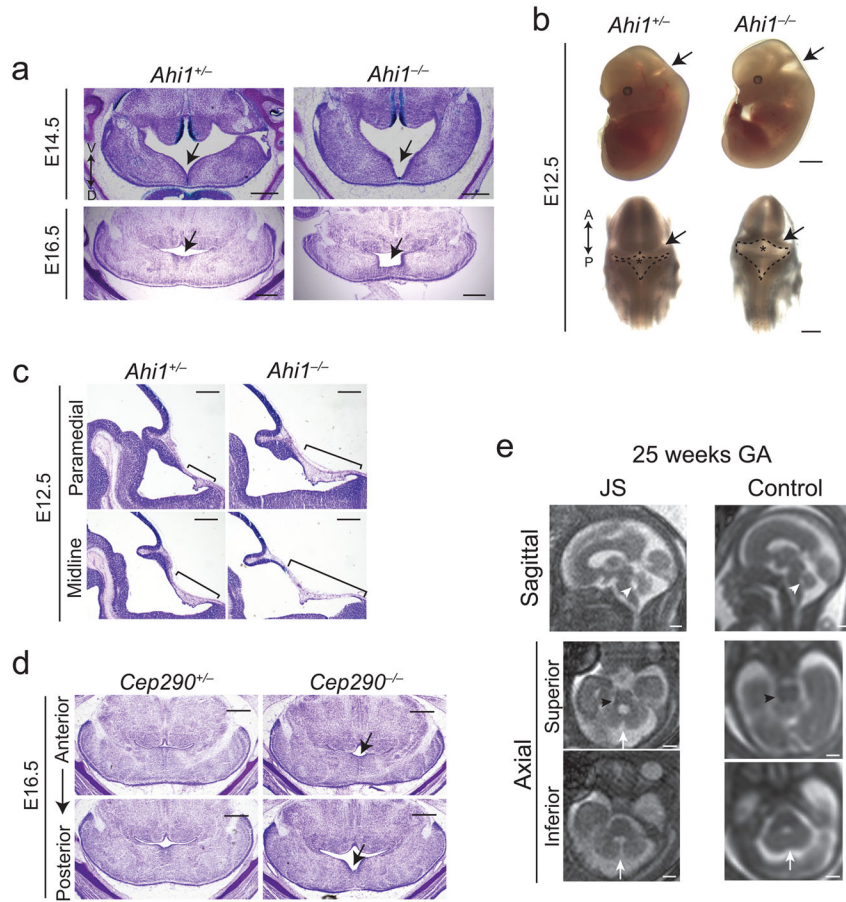


Figure 3. Midline fusion defect in mice and humans with Joubert syndrome

(a) Transverse C-V stained sections from littermates at E16.5 and E14.5 revealing midline fusion defect (arrows). Scale bar, 0.5 mm. (b) Whole mount images of littermate embryos at E12.5 imaged laterally (top) and dorsally (bottom). Arrows point to the expanded roof plate and fourth ventricle. Dashed lines demarcate roof plate while asterisks point to cerebellar vermis anlage. Anterior (A) and posterior (P) directionality is depicted by a double arrow. Scale bar, 2 mm (upper panels), 1 mm (lower panels). (c) Midline and medial sagittal C-V stained sections from E12.5 littermates revealing elongated roof plate (bars). Scale bar, 0.5 mm. (d) Transverse cresyl-violet stained sections of representative *Cep290* mutant and littermate control embryos at E16.5. Arrows point to mild midline fusion defect, which is more pronounced on posterior sections. Scale bar, 0.5 mm. (e) Fetal MRIs from a representative subject with Joubert syndrome and a control fetus both 25 weeks gestational age (GA). Sagittal image reveals superiorly tilted fourth ventricle roof (white arrowhead), while axial series reveals a gap between cerebellar hemispheres (arrows) that is more severe on inferior sections. The MTI is also already visible in the fetus with Joubert syndrome (black arrowhead). Scale bar, 1 cm.

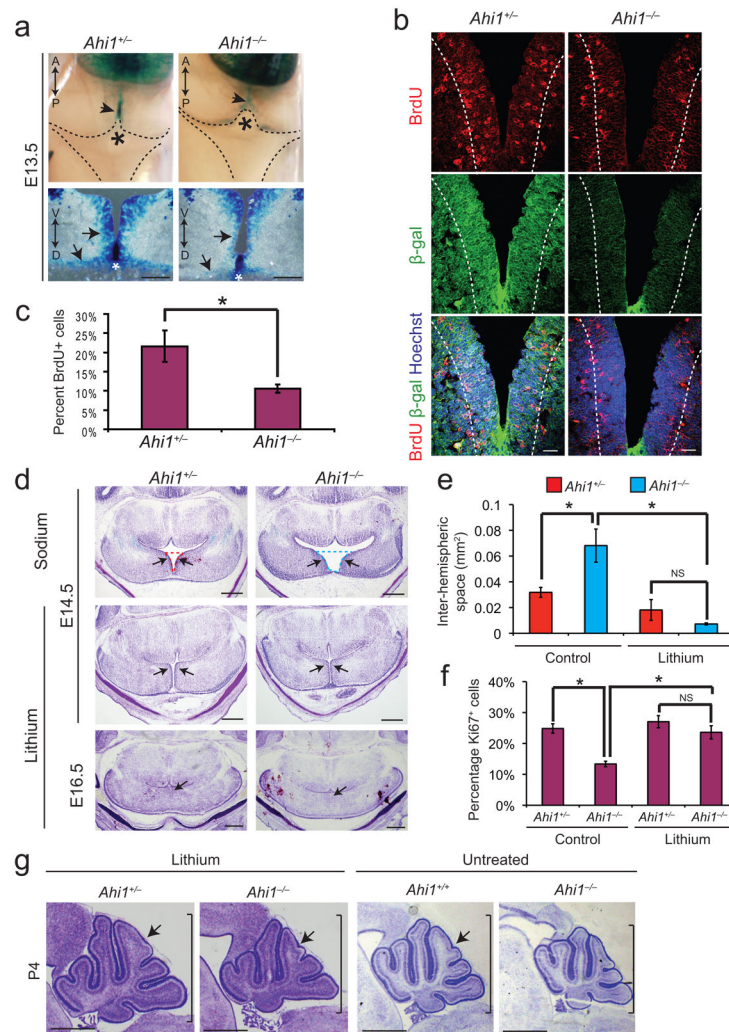


Figure 4. Defective Wnt signaling and lithium rescue in *Ahi1* mutant cerebella

(a) Top, X-gal stained whole mount dorsal view of E13.5 BATgal+ littermates revealing Wnt activity (arrowheads) at the site of hemisphere fusion (asterisk). Bottom, X-gal stained transverse sections of superior cerebellar anlage from BATgal+ littermates. White asterisks depict roof plate directly abutting the site of midline fusion. Arrows point to cerebellar hemisphere cells surrounding the midline with decreased Wnt activity and defective fusion in *Ahi1* null. Scale bar, 100 μ m. (b) β -galactosidase (green) and BrdU (red) antibody staining of transverse superior cerebellar sections of *Ahi1* null and littermate control BATgal+ embryos at E13.5. Dashed line indicates the five-cell layer boundary used for BrdU counting in c. Hoechst (blue) labels nuclei. Scale bar, 20 μ m. (c) Quantification of BrdU positive cells adjacent to ventricle relative to total cell number as determined by Hoechst. * $P < 0.05$, Student's *t*-test, $n = 3$ for each genotype. Error bars are S.E.M. (d) C-V stained transverse sections of *Ahi1* mutant and littermate control embryos. First row: E14.5 control NaCl treated littermates. Dashed lines represent measurement area for panel e. Second row: E14.5 LiCl treated mutant and control littermates. Arrows point to expansion of cerebellar hemispheres. Third row: E16.5 LiCl treated mutant and control littermates with complete

midline fusion (arrows). Scale bar, 0.5 mm. (e) Degree of separation of cerebellar hemispheres as measured by average inter-hemispheric space. $*P < 0.05$, Student's *t*-test, $n = 3$ for each genotype (littermates) and condition. Error bars are S.E.M. NS=not significant. (f) Average percentage of Ki67⁺ cells relative to total cell number (Hoechst). $*P < 0.05$, Student's *t*-test, $n = 3$ for each genotype (littermates) and condition. Error bars are S.E.M. NS=not significant. (g) Sagittal C-V stained sections from P4 *Ahi1* mutants and littermate controls from a dam treated with LiCl or untreated. Note the similarity between *Ahi1*^{-/-} treated with LiCl (second panel) to untreated *Ahi1*^{+/+} (third panel). Scale bar, 1 mm.